

Comprehensive inelastic neutron scattering study of the multiferroic $\text{Mn}_{1-x}\text{Co}_x\text{WO}_4$

Jinchen Wang,^{1,2} R. S. Fishman,³ Yiming Qiu,⁴ J. A. Fernandez-Baca,² Georg Ehlers,⁵ K.-C. Liang,⁶ Yaqi Wang,⁶ Bernd Lorenz,⁶ C. W. Chu,^{6,7} and Feng Ye^{2,*}

¹Department of Physics, Renmin University of China, Beijing 100872, China

²Neutron Scattering Division, Oak Ridge National Laboratory, Oak Ridge, Tennessee 37831, USA

³Materials Science and Technology Division, Oak Ridge National Laboratory, Oak Ridge, Tennessee 37831, USA

⁴NIST Center for Neutron Research, National Institute of Standards and Technology, Gaithersburg, Maryland 20899, USA

⁵Neutron Technologies Division, Oak Ridge National Laboratory, Oak Ridge, Tennessee 37831, USA

⁶Department of Physics and TCSUH, University of Houston, Houston, Texas 77204, USA

⁷Lawrence Berkeley National Laboratory, 1 Cyclotron Road, Berkeley, California 94720, USA



(Received 17 September 2018; revised manuscript received 20 November 2018; published 14 December 2018)

Using high-resolution inelastic neutron scattering, we examine the spin dynamics of $\text{Mn}_{1-x}\text{Co}_x\text{WO}_4$ in the collinear AF1, the *ac-b* spiral AF2, and the *ac* cycloidal AF5 phases. The spin wave excitations are well described by a Heisenberg model with competing long-range exchange interactions (J_i up to 12th nearest neighbors) and the single-ion anisotropy K induced by the spin-orbit interaction. While the exchange constants are relatively unchanged, the dominant effect of doping is to change the single-ion anisotropy from easy axis ($K > 0$) in the collinear AF1 phase to easy plane ($K < 0$) in the two multiferroic phases.

DOI: [10.1103/PhysRevB.98.214425](https://doi.org/10.1103/PhysRevB.98.214425)

I. INTRODUCTION

There has been a long pursuit for materials exhibiting coupled magnetic and electric properties for both their technological and fundamental scientific interest. Inspired by the magnetic control of ferroelectric polarization in TbMnO_3 [1], considerable work has focused on type-II multiferroic materials where ferroelectricity has a magnetic origin [2–6]. A type-II multiferroic can be realized through the spin-current or inverse Dzyaloshinskii-Moriya (DM) interaction [7–9], exchange striction [10], or *p-d* hybridization [11,12]. Due to the delicately balanced ground states in these materials, noncollinear spin structures are often produced by magnetic frustration and competing interactions. Consequently, their electric or magnetic properties can be easily tuned by external perturbations.

Multiferroic MnWO_4 is a classic example of a frustrated magnet with coupled electric and magnetic properties [13–15]. It crystallizes in the monoclinic hübnerite structure (space group $P2_1/c$, No. 13), where edge-sharing MnO_6 octahedra form zigzag chains along the *c* axis [Fig. 1(a)]. Upon cooling, MnWO_4 undergoes successive magnetic transitions [16]. Below 13.5 K, the incommensurate (ICM) AF3 phase has a collinear sinusoidal structure with a magnetic wave vector that depends on temperature T . An ICM AF2 phase is stabilized when $12 > T > 7$ K with the wave vector locked at $\mathbf{q} = (-0.214, 1/2, 0.457)$. This phase hosts a spiral magnetic structure that breaks inversion symmetry [17] and supports a spontaneous electric polarization along the *b* axis that is explained by the spin-current mechanism. Below 7 K, the electric polarization disappears upon formation of the com-

mensurate AF1 phase, which has a collinear $\uparrow\downarrow\downarrow\downarrow$ configuration with wave vector $\mathbf{q} = (-1/4, 1/2, 1/2)$. This collinear state can be destabilized by various perturbations, including magnetic field [13,18–21], chemical doping [22–27], and pressure [28].

Among all magnetic and nonmagnetic chemical substitutions, Co-doped MnWO_4 exhibits the most complex magnetic properties [29–35]. Only a few percent Co doping ($x > 0.02$) suppresses the AF1 structure completely and stabilizes the AF2 phase. This situation is similar to the triangular lattice CuFeO_2 where Al or Ga doping drives the system into a multiferroic spin-spiral phase [36,37]. Further Co doping ($x > 0.075$) changes the spin structure into an *ac* cycloidal configuration (AF5 phase with spins in the *ac* plane) accompanied by a polarization flop from the *b* axis into the *ac* plane [29,34]. When $x > 0.15$, the polarization reverts to the *b* axis, and the spins form a conical structure [29,33].

A number of microscopic mechanisms have been proposed to explain this complex phase diagram. The successive changes of the magnetic and electric polarization states may be caused by the higher-order coupling between the polarization (\mathbf{P}) and magnetic (\mathbf{M}) order parameters in the form of $\gamma \mathbf{P} \cdot [\mathbf{M}(\nabla \cdot \mathbf{M}) - (\mathbf{M} \cdot \nabla)\mathbf{M}]$ [38]. As supported by the distinct phase diagrams for different magnetic dopants [22,24,26,27], the competing magnetic anisotropy of the Mn and Co ions may also be relevant [39,40]. It has been proposed that the consecutive spin-flop transitions and the appearance of the noncoplanar, conical spin state at higher Co concentrations are explained by the biquadratic exchange interaction $B_{ij}(\mathbf{S}_i \cdot \mathbf{S}_j)^2$ between Mn and Co ions, which is expected to be stronger between Mn^{2+} ($3d^5$ electronic configuration) and Co^{2+} ($3d^7$ state) than the magnetic ions of the same type [40]. Finally, due to its relatively smaller ionic size (0.745 Å for Co^{2+} versus 0.83 Å for Mn^{2+}), the substitution of Co^{2+}

*yef1@ornl.gov

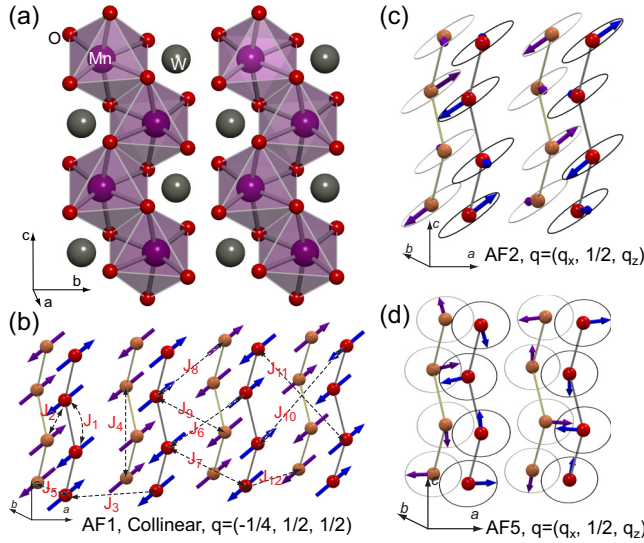


FIG. 1. (a) The crystal structure of $\text{Mn}_{1-x}\text{Co}_x\text{WO}_4$. The spin structures of (b) the collinear commensurate (CM) AF1 phase (magnetic point group $2/m1'$) with spins in the ac plane at an angle of $\sim 35^\circ$ to the a axis, (c) the noncollinear ICM AF2 phase ($21'$) with one elliptical spiral axis in the ac plane and the other along the b axis, and (d) the noncollinear ICM AF5 phase ($m1'$) with the spin cycloid in the ac plane. (The spin configuration plots are from previous publication of Ref. [29].) In (b), we label the magnetic interactions with increasing Mn-Mn bond distances.

introduces chemical pressure, which is an important tuning parameter in many magnetically frustrated systems.

The key questions are as follows: What is the dominant effect of chemical substitution, and how do impurities alter the phase diagram? Based on the above discussion, several scenarios can explain the changes in the magnetic configuration. (1) Doping could preferentially change one exchange coupling compared to the rest, thereby enhancing or reducing magnetic frustration. (2) Chemical substitution could introduce extra exchange pathways not present in the pure compound. (3) Doping could introduce additional types of interactions, like DM interactions due to broken inversion symmetry or biquadratic superexchange interactions arising from the higher-order terms in the exchange integral or the orbital overlap [41]. (4) Chemical substitution could alter the existing anisotropy, freeing the spins to form a spiral state.

Using high-resolution inelastic neutron scattering (INS), we have investigated the spin dynamics of $\text{Mn}_{1-x}\text{Co}_x\text{WO}_4$ in the AF1 ($x = 0$, $T = 1.4$ K), AF2 ($x = 0$, $T = 8.5$ K), and AF5 ($x = 0.12$, $T = 1.4$ K) phases. An analysis of the magnetic dynamics reveals that the effect of chemical substitution involves mechanisms (3) and (4) listed above. The same basic model that describes the AF1 phase of the pure compound also describes the AF5 phase of the doped compound, except that the single-ion anisotropy has changed sign from the easy axis located in the ac plane ($K > 0$) to the easy plane ($K < 0$) normal to the b axis. In the AF2 phase, additional DM interactions might also play an important role.

Single crystals of $\text{Mn}_{1-x}\text{Co}_x\text{WO}_4$ ($x = 0$ and 0.12) were grown using the floating-zone technique. Chemical compositions were independently verified by energy-dispersive

x-ray measurements and neutron diffraction refinement. High-resolution INS measurements were performed using the Disk Chopper spectrometer at the NIST Center for Neutron Research [42] and the Cold Neutron Chopper Spectrometer at the Spallation Neutron Source at Oak Ridge National Laboratory (ORNL) [43]. The momentum transfer \mathbf{q} is expressed as (H, K, L) in reciprocal lattice units (r.l.u.) such that $\mathbf{q} = H\mathbf{a}^* + K\mathbf{b}^* + L\mathbf{c}^*$, where \mathbf{a}^* , \mathbf{b}^* , and \mathbf{c}^* are the reciprocal lattice vectors. The crystals were aligned primarily in two different scattering planes so that the spin-wave (SW) dispersions along the $[1, 0, -2]$, $[1, 0, 2]$, and $[0, 1, 0]$ symmetric directions can be measured. The data analysis and visualization were processed using the DAVE software package [44]. To resolve the SW branches, we chose incident neutrons with a wavelength of $\lambda = 4.4$ Å and energy resolution $\Delta E \approx 0.1$ meV. The sample temperature was regulated using a liquid-helium cryostat.

The SW frequencies and intensities are calculated based on the general Heisenberg Hamiltonian:

$$H = -\frac{1}{2} \sum_{i,j} J_{ij} \mathbf{S}_i \cdot \mathbf{S}_j - K \sum_i S_{iz}^2, \quad (1)$$

where $\sum_{i,j}$ indicates the summation over pairs of spins, J_{ij} are the superexchange (SE) couplings, and K is the single-ion anisotropy, with $K > 0$ denoting the spin components along the easy axis and $K < 0$ indicating the spins are in the easy plane. The spin configuration is obtained from the static magnetic structure refinement and is used to calculate the magnetic scattering cross section with the form

$$\frac{d^2\sigma}{d\Omega dE} \propto f^2(|\mathbf{q}|) e^{-2W} \sum_{\alpha\beta} (\delta_{\alpha\beta} - \hat{q}_\alpha \hat{q}_\beta) S^{\alpha\beta}(\mathbf{q}, \omega), \quad (2)$$

where $f^2(|\mathbf{q}|)$ is the magnetic form factor for the Mn^{2+} ion, e^{-2W} is the Debye-Waller factor, $\delta_{\alpha\beta}$ is the Kronecker delta, \hat{q}_α is the α component of a unit vector in the direction of \mathbf{q} , and $S^{\alpha\beta}(\mathbf{q}, \omega)$ is the response function that describes the $\alpha\beta$ spin-spin correlations [45,46]. We also emphasize that the effective Hamiltonian is used for both the pure and doped MnWO_4 since the small number of Co ions are uniformly distributed at the Mn sites and a description using averaged exchange interaction constants and anisotropy is justified.

II. SPIN WAVES IN THE COLLINEAR AF1 PHASE

We first revisit the SW spectra of undoped MnWO_4 in Figs. 2(a)–2(c). These scans are along the high-symmetry $[1, 0, -2]$, $[1, 0, 2]$ and $[0, 1, 0]$ directions. Since the magnetic unit cell of the collinear phase contains eight Mn spins (four spin up and four spin down), diagonalization of the 16×16 magnetic Hamiltonian matrix produces four SW branches (each twofold degenerate). The data clearly show distinct branches dispersing out from the magnetic zone center (ZC) to the zone boundary (ZB). The spectra reveal a ZC spin gap of 0.5 meV and a ZB energy of around 2.2 meV. The excitation bandwidth is consistent with the energy scale of the ordering temperature of 13.5 K. The intensities of the excitation spectra are highly asymmetric with respect to the magnetic Bragg points, as seen in the lowest branch in both Figs. 2(a) and 2(b).

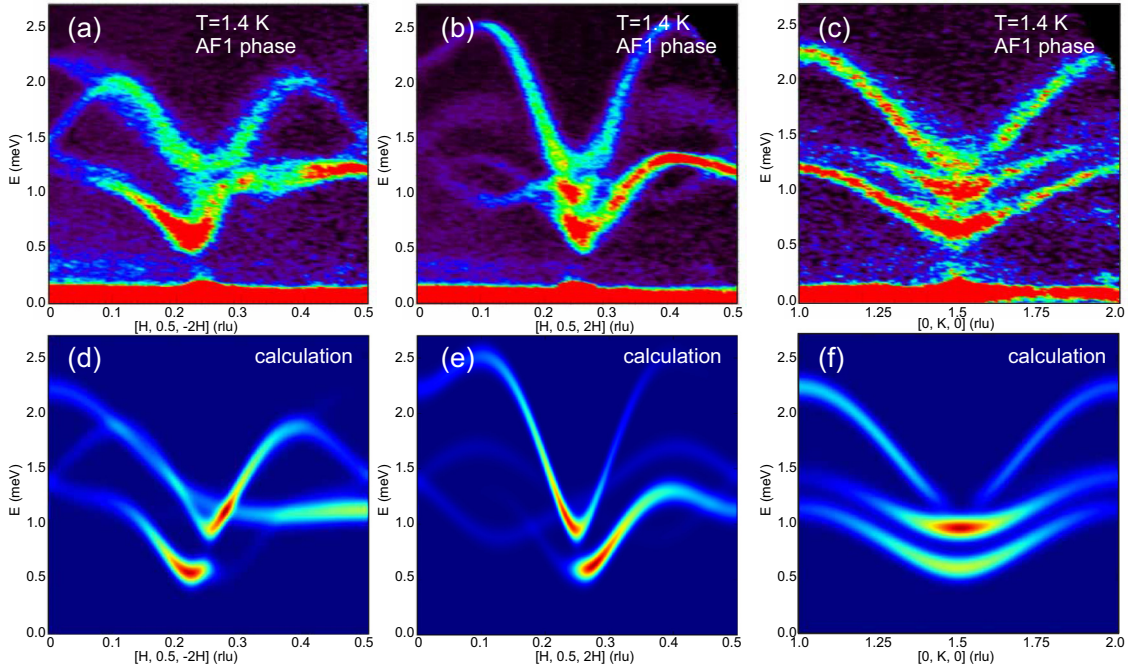


FIG. 2. SW dispersion spectra of pure MnWO_4 along the (a) $[1, 0, -2]$, (b) $[1, 0, 2]$, and (c) $[0, 1, 0]$ directions in the commensurate $\uparrow\uparrow\downarrow$ AF1 phase. (d)–(f) The corresponding SW spectra calculated using the exchange parameters listed in Table I.

This indicates that sufficient coverage in reciprocal space is necessary to fully characterize the magnetic dynamics.

Although our previous analysis using exchange interactions up to 11th nearest neighbors captured the essential features of the SW spectra in the collinear phase, there were some minor disagreements between the calculated spectral weight and experimental observations. For example, the lowest branch along $[1, 0, -2]$ was predicted to have significant scattering intensity for $H > 0.25$, which was not observed experimentally (Fig. 3(c) of Ref. [47]).

We have reanalyzed the SW dynamics of the AF1 phase using improved numerical techniques [46]. Including exchange interactions up to J_{12} , the dispersion relation and the spectral intensity in Fig. 2(d) nicely reproduce the experimental data shown in Fig. 2(a). The refined exchange parameters and the single-ion anisotropy K are listed in Table I. Our results are consistent with the independent INS work by Xiao *et al.* [48], where the subtle difference is likely due to the uncertainty in extracting the dispersion relations from the experimental data.

Recently, calculations based on SE theory were employed to investigate the spin configurations and the electric polariza-

tion in MnWO_4 [49]. When the low-energy model is solved in the mean-field Hartree-Fock approximation without taking into account the relativistic spin-orbit interaction (SOI), all the SE parameters J_i (up to J_{12}) obtained from the calculation are in good agreement with the experimentally derived results reported here and in Ref. [48]. This underscores that the long-range isotropic exchange interactions are necessary to stabilize the magnetic structure. However, the balance between the J_i alone cannot explain the orientation of the spins in the ac plane in the AF1 phase, nor can it explain the inversion symmetry breaking responsible for the b -axis polarization in the AF2 phase. The relativistic SOI introduces critical ingredients such as the single-ion anisotropy and DM interactions.

Solovyeu [49] studied the effect of single-ion anisotropy K on the spin texture in the AF1 phase in the atomic limit with transfer integrals set to zero. The presence of K aligns the spins either parallel to the b axis or in the ac plane due to the symmetry operators of the $P2/c$ space group. The configuration obtained has spins canting 41° off the a axis, close to the experimental observation. Moreover, the estimated DM terms in the collinear phase are roughly of the

TABLE I. Magnetic exchange coupling parameters derived from the SW model calculation for the collinear AF1 phase and the noncollinear AF2 and AF5 phases. The bonding distances (in Å) between $\text{Mn} \cdots \text{Mn}$ are also listed. The magnetic interaction constants have been normalized in units of meV. For comparison, the parameters in Refs. [47,48] are given in $J_i S$ and $K S$ with $S = 5/2$.

	J_1	J_2	J_3	J_4	J_5	J_6	J_7	J_8	J_9	J_{10}	J_{11}	J_{12}	K	χ^2
Mn \cdots Mn	3.286	4.398	4.830	4.990	5.760	5.801	5.883	6.496	6.569	6.875	7.013	7.520		
AF1 (Ref. [48])	-0.148	-0.001	-0.068	-0.084	-0.004	-0.136	-0.044	-0.004	-0.080	-0.048	-0.017	-0.006	0.024	
AF1 (this work)	-0.191	-0.025	-0.099	-0.112	-0.006	-0.158	-0.060	-0.007	-0.098	-0.064	-0.016	-0.016	0.032	1.61
AF2 (this work)	-0.200	-0.015	-0.096	-0.079	0.020	-0.182	-0.053	0.013	-0.073	-0.082	-0.023		-0.034	3.01
AF5 (this work)	-0.241	-0.078	-0.111	-0.117	-0.032	-0.161	-0.074	-0.013	-0.093	-0.083	-0.034		-0.011	2.67

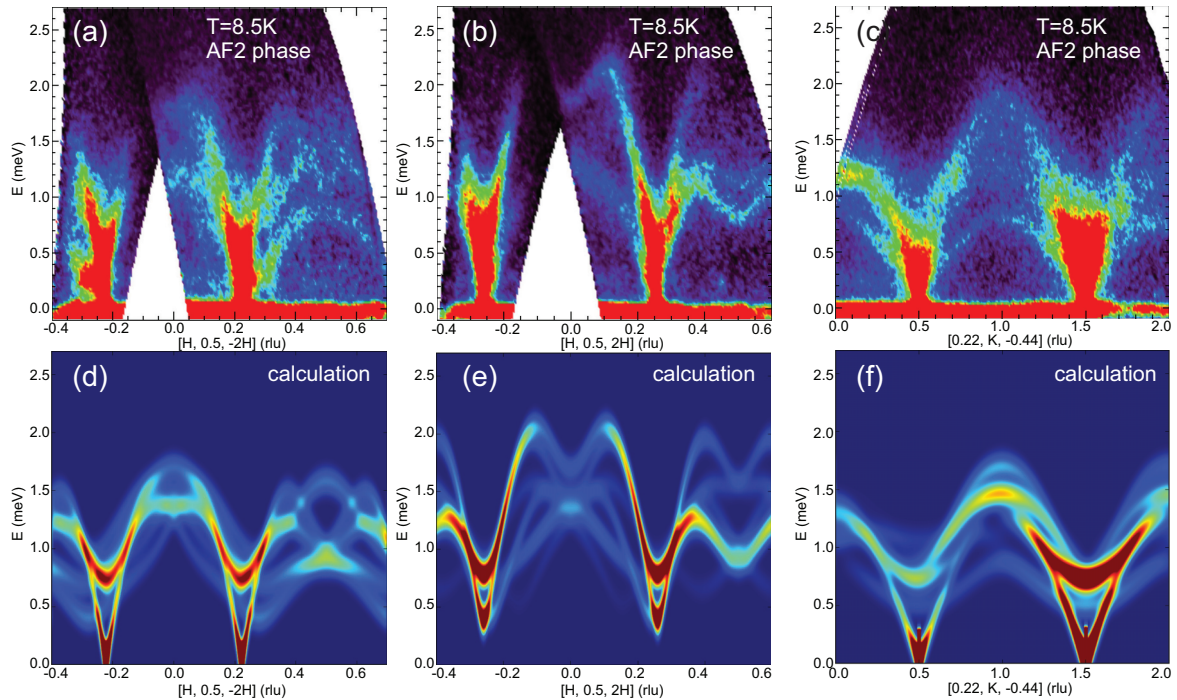


FIG. 3. SW dispersion spectra of pure MnWO_4 along (a) the $[1, 0, -2]$, (b) $[1, 0, 2]$, and (c) $[0, 1, 0]$ directions in the incommensurate AF2 phase with ac - b spiral spin structure at $T = 8.5$ K. (d)–(f) The corresponding SW spectra calculated using the exchange parameters listed in Table I.

order of $DS^2 \approx 0.01$ meV or $D \approx 0.0016$ meV. These DM interactions produce an additional canting of the spin out of the ac plane. The applied force alternates on individual spins of the same magnetic sublattice because of the $\uparrow\uparrow\downarrow\downarrow$ configuration. Thus, the isotropic exchange interactions, single-ion anisotropy, and DM interactions work cooperatively to stabilize the AF1 phase (which we shall still call collinear despite its slight distortion). Meanwhile, inversion symmetry is preserved, and the polarization is absent in the AF1 state. As we will see in the following, that is not the case for the spiral AF2 phase.

III. SPIN WAVES IN THE SPIRAL AF2 PHASE

As the temperature increases, the magnetic structure transforms from the collinear AF1 phase to the spiral AF2 phase. The two principal axes of the spiral lie in the ac plane and along the b axis, respectively [16]. We measured the SW spectra of undoped MnWO_4 in the AF2 phase at $T = 8.5$ K. Figures 3(a)–3(c) show the evolution of the magnetic dynamics when the spin structure is in the ac - b spiral phase. Compared to Figs. 2(a)–2(c) for the AF1 phase, the most prominent change is that the SW gap is nearly absent within instrumental resolution. In addition, the spectra in the AF2 phase are no longer as well resolved as in the collinear AF1 state, and the spectral intensities are considerably redistributed along different symmetry directions. For example, the lowest branch with energy transfer ΔE between 0.8 and 1.0 meV in Fig. 3(b) shows the largest spectral weight for $0.4 < H < 0.6$, which contrasts with the data in Fig. 2(b), where the second branch with energy transfer ΔE between 1.0 and 1.2 meV shows the

stronger scattering signal. The difference clearly demonstrates the change in the spin Hamiltonian.

To obtain a faithful characterization of the magnetic dynamics, we extracted the SW dispersion curves, which have significant spectral weight and are well separated from the nearby branches. Since the AF2 phase possesses an ICM structure, we chose the magnetic wave vector $\vec{q}_m = (-2/9, 1/2, 4/9)$ that is close to the measured $(-0.214, 1/2, 0.457)$. The computation load is significantly reduced as we need to diagonalize only a 72×72 matrix (where $72 = 9 \times 8$) for each momentum transfer. Eigenvalues with significant weight are used to produce the plots in Figs. 3(d)–3(f).

Although the experimental spectra of the AF2 phase bear quite different features, the coupling constants J_i are close to the AF1 phase. We limited our calculation with J_i up to the 11th nearest neighbor as inclusion of J_{12} does not yield further improvement. Moreover, the sign of the anisotropy term K changes from positive to negative. It reveals that the spin anisotropy switches from an easy axis to an easy plane. One also notices that spectra produced using the Hamiltonian in Eq. (1) have some discrepancies with the experimental observation, implying the model involving only J_i and K might not be sufficient to capture all the dynamical details and may have to consider other terms, including the SOI.

It was pointed out that an undistorted spiral magnetic structure is not consistent with a ferroelectric polarization. Although the spatial inversion seems to be broken in a homogenous spin-spiral texture, the original spin configuration can always be recovered by a universal 180° rotation of every spin around the axis parallel to $e + \hat{I}e$, where e is the spin direction at the specific site and $\hat{I}e$ is the spin direction at

the same site after the inversion operation of the lattice [49]. This argument indicates the ferroelectricity exists only in the deformed spin-spiral state due to SOI, i.e., DM interaction. Because the DM vectors $\mathbf{d}_{R'}$ lie in the ac plane, the forces exerted on the spins in the ac plane will rotate the spins within that plane due to the cross product between the DM vectors and the spins in the form of $\mathbf{d}_{R'} \times \mathbf{e}_{R+R'}$. Furthermore, the forces applied to the Mn1 and Mn2 sublattices have opposite directions; this causes the spiral planes of individual Mn1 and Mn2 sublattices to tilt in different directions.

Recent single-crystal neutron diffraction using the super-space group formalism reveals that the spin configuration in the AF2 phase is indeed a deformed spiral [17]. The spin state arises from the activation of two irreducible representations (irreps), where the magnetic supergroup is reduced to $P21'(\alpha, 1/2, \gamma)0s$. Because the two magnetic ions Mn1 and Mn2 located at $(1/2, 0.685, 1/4)$ and $(1/2, 0.315, 3/4)$ in the unit cell are no longer related by an inversion center, their moments can be refined independently. The remaining twofold rotation operator along the b axis leaves each Mn_i atom unchanged. This dictates stringent constraints on the moment direction; the a and c spin components are proportional to a cosine modulation, while the b component is proportional to a sine one. Thus, the moments in the AF2 form an ellipse with the two principal axes lying in the ac plane and along the b axis, respectively. The long axis moment m_{ac} is approximately $3.9\mu_B$, and the short one m_b is $\sim 3.1\mu_B$ [17]. In addition, the normal axes of the two spiral planes tilt away from the c axis differently, with angles 37.2° and 29.8° for the Mn1 and Mn2 sublattices, respectively. Both features imply that the spin order in the AF2 phase shows appreciable deformation from a circular spiral and forms a noncoplanar superposition of two ellipses.

Combining the measured spin wave and the static spin configuration, it becomes evident that the SOI changes significantly both the dynamic and static channels in the multiferroic AF2 phase and plays a key role in coupling the electric to the magnetic properties.

IV. SPIN WAVES IN THE CYCLOIDAL AF5 PHASE

The substitution of Co ions in $\text{Mn}_{1-x}\text{Co}_x\text{WO}_4$ causes two consecutive spin-state transitions. The AF1 phase transforms into the noncollinear AF2 phase when $x > 0.02$ with its spiral axis in the ac plane and then to a cycloidal AF5 phase with the normal axis to the cycloidal plane along the b direction when $0.15 > x > 0.075$.

In contrast to the AF2 phase, the spin state of the AF5 phase is the superposition of two identical irrep magnetic modulations with a constant phase shift of $\pi/2$ or $3\pi/2$ between the two. The magnetic superspace group becomes $Pm1'(\alpha 1/2 \gamma)0s$, and the magnetic point group is $m1'$ [Fig. 1(d)]. This point group permits the appearance of an electric polarization in the ac plane. Neutron diffraction reveals that the cycloidal configuration is again deformed; the moment along the long axis of the ellipse m_a is larger than the one along the short axis m_c [29]. Electric polarization along both the a and c axes was observed [38].

As discussed earlier, multiple mechanisms are capable of explaining the complex phase diagram. INS is probably the

most effective tool to characterize the evolution of the interactions and to clarify the nature of the spin-state transitions. We chose $x = 0.12$ for the INS study since a sample with this concentration does not exhibit the gradual change in magnetic wave vector like for the lower doping of $x = 0.1$ or the coexistence of multiple competing magnetic phases like for the higher doping of $x = 0.15$ [29,32]. Instead, sequential AF3 \rightarrow AF1 \rightarrow AF5 phase transitions are observed as the $x = 0.12$ sample is cooled to the base temperature. Once the system enters the ac cycloidal phase, the propagation wave vector remains constant, indicating that the AF5 phase is stable against the thermal fluctuation.

Figures 4(a)–4(c) show the SW dynamics of the AF5 phase in $\text{Mn}_{0.88}\text{Co}_{0.12}\text{WO}_4$ along the same directions as in Figs. 2 and 3. Subtle differences between the SW spectra of the AF2 and AF5 phases are visible. The dispersion curves in the AF5 phase are rather sharp, which allows a reasonable extraction of the dominant SW branches. Using an approach similar to that in the AF2 phase, we have expanded the magnetic cell with a wave vector $(3/13, 1/2, -6/13)$ that is close to the experimentally determined $(0.22, 1/2, -0.48)$ [29]. The calculation then requires the diagonalization of a 104×104 matrix (where $104 = 13 \times 8$) for each momentum transfer. The best-fit parameters listed in Table I show that the change in the exchange interactions J_i remains minor, while the single-ion anisotropy $K < 0$ has the same sign as in the AF2 phase. The negative value of K again implies that the spins prefer to lie in an easy plane. The calculated SW spectra in Figs. 4(d)–4(f) fit the measurements nicely along all symmetry directions.

To validate the results, we calculate the total energies for the AF1 and AF5 configurations using the experimentally determined exchange parameters in the AF5 phase. The energy associated with the AF1 phase (-3.942 meV/site) is higher than that of the AF5 state (-3.997 meV/site). The energy difference per site for AF1 to AF5 is 0.64 K and corresponds to a total energy of 5.1 to 10.2 K for a magnetic domain consisting of 8 – 16 spins. This agrees well with the observed transition from the AF1 to the AF5 phases as the $x = 0.12$ sample is cooled [29].

V. DISCUSSION

A systematic study of the spin dynamics allows us to correlate the evolution of the interaction parameters with the static magnetic and electric polarization properties. Figure 5 summarizes the distance dependence of the J_i for the different magnetic phases. Although the magnetic configurations are quite different, there are several common features among the three spin states: The overall spin-spin exchange interactions are relatively unchanged. Longer-range couplings are required to stabilize the spin order. The next-neighbor antiferromagnetic interaction J_1 remains the strongest one, and the small interchain interaction J_5 is insensitive to the spin states.

In the collinear AF1 phase, the spin texture is mainly stabilized by the competing isotropic exchange interactions. The spatial orientation of the moments in the collinear phase is driven by the single-ion (easy-axis) anisotropy. The easy axis lying in the ac plane is dictated by the symmetry operators of the space group $P2/c$. The single-ion anisotropy

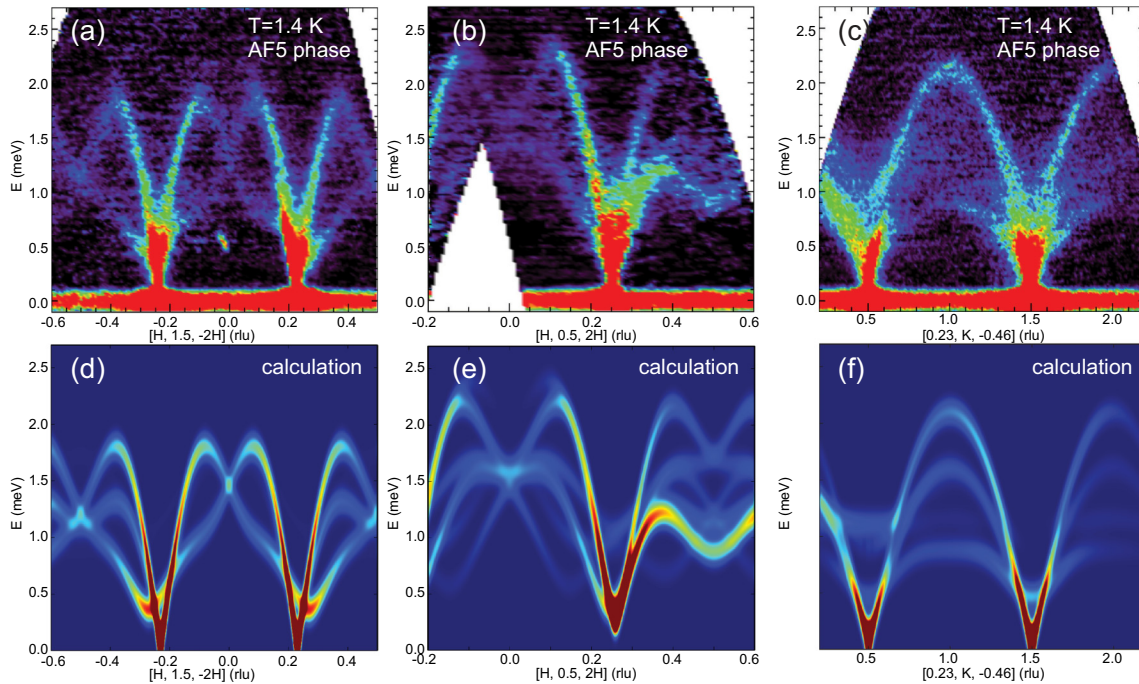


FIG. 4. (a) SW spectra of $\text{Mn}_{0.88}\text{Co}_{0.12}\text{WO}_4$ along (a) the $[1, 0, -2]$, (b) $[1, 0, 2]$, and (c) $[0, 1, 0]$ directions in the incommensurate AF5 phase with an ac cycloidal spin configuration. (d)–(f) The corresponding SW spectra calculated using the exchange parameters listed in Table I.

$K = 0.032$ meV obtained from the SW calculation is ten times smaller than the energy scale of the strongest J_i . We emphasize that isotropic magnetic exchange interactions together with the single-ion anisotropy K are sufficient to describe the SW dynamics of the AF1 phase. Since the theoretically estimated DM interactions $D \approx 0.0016$ meV are much smaller than $K \approx 0.03$ meV, they are not expected to significantly improve the fits in the AF1 phase. An electric polarization is absent in this phase because the spatial inversion symmetry is preserved by all possible interactions.

SW studies of $\text{Mn}_{0.88}\text{Co}_{0.12}\text{WO}_4$ in the AF5 phase show that the overall isotropic exchange interactions are similar to

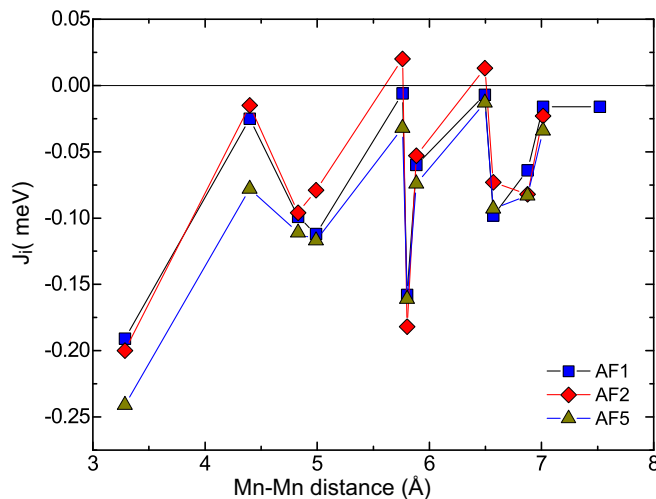


FIG. 5. The distance dependence of the isotropic exchange interactions in the AF1, AF2, and AF5 phases. The corresponding Mn-Mn distances are displayed in Fig. 1.

those in the parent compound. Hence, structural modifications due to the size of Co ions do not lead to an appreciable change to the interaction strength. However, the distinct single-ion character of Co^{2+} ions does rotate the spins into the ac plane. Compared to the collinear AF1 phase, the single-ion anisotropy K is reduced in the AF5 phase. The suppression of the easy-axis anisotropy with a small amount of chemical substitution is consistent with the observation in other multiferroic systems. For instance, the spin dynamics of the triangular lattice antiferromagnet $\text{CuFe}_{0.965}\text{Ga}_{0.035}\text{O}_2$ shows gapless excitation at the zone center, in contrast to a finite spin gap for undoped CuFeO_2 [50]. Fits to the SW spectra of pure and doped $\text{CuFe}_x\text{Ga}_{1-x}\text{O}_2$ reveal that the easy-axis anisotropy K decreases from 0.22 to 0.01 meV.

A complete model for pure and doped MnWO_4 should include both the DM and single-ion anisotropy terms. A good description of the spin dynamics in the AF1 and AF5 phases based on a spin Hamiltonian with only K indicates that the DM terms of the order of 0.0016 meV cause small corrections in those phases. For the AF1 phase, $K = 0.032$ meV, while for the AF5 phase, $K = -0.011$ meV. If there is a systematic suppression of K upon Co doping, then K will vanish at a certain point when the system evolves from the AF1 to the AF5 phase. Although the DM interaction is negligible in the AF1 and AF5 phases, it might make a significant contribution when the doped system is close to the phase boundary, where D is comparable to $|K|$ and although the value of D is small.

In fact, the larger-than-expected value of $|K| \approx 0.034$ meV and the sign reversal in the AF2 phase may compensate for the incompleteness of our model, i.e., the absence of the DM term. A better estimate for K in the AF2 phase would then require that we include both the K and DM terms and construct the appropriate distorted spin structure stabilized

by those parameters. Our model containing only isotropic exchange and single-ion anisotropy yields a less satisfactory fit to the spin dynamics of the AF2 phase ($\chi^2 \approx 3$) than of the AF1 ($\chi^2 \approx 1.6$) and AF5 ($\chi^2 \approx 2.7$) phases. It is also worth noting that the spin dynamics of the AF2 phase is measured at elevated temperature in the undoped MnWO₄, which might exhibit different character than the AF2 phase that is induced by a small amount of Co substitution. Nevertheless, the spin spiral of the AF2 phase is more distorted than that of the AF5 phase. It would be interesting to carry out a more sophisticated analysis of the AF2 phase that includes both the anisotropy and DM interactions. A similar approach was employed by Chun *et al.* to explain the blueshift of the electromagnon in the multiferroic hexaferrite [51], where the DM term in the effective Hamiltonian is believed to play a critical role in the dynamical magnetoelectric effect.

The importance of the SOI in these compounds is beyond dispute [49]. Generally, the mechanism that produces a non-collinear state can be distinct from the mechanism that couples the noncollinear state to electrical properties. Although competing long-range exchange interactions produce the non-collinear states of the AF2 and AF5 phases, the isotropic exchange coupling cannot lead to the observed ferroelectric behavior. In type-II multiferroics, both the spin-current model and the spin-dependent *p-d* hybridization mechanism involve the SOI for the spiral-type spin order [6–12]. The influence of SOI that significantly distorts the spiral spin states can be seen most clearly in the AF2 phase. For all three phases (AF1, AF2, and AF5), the exchange interactions are almost comparable. So in the absence of the SOI, the “natural” spiral or cycloidal states of the AF2 and AF5 phases would be almost the same, with wave vectors $\sim(0.22, -0.5, 0.46)$. The distinction between the spin states of the AF1, AF2, and AF5 phases is largely due to the difference of SOI-induced anisotropy *K* and perhaps to a lesser extent to the DM interactions.

One goal of work on doped MnWO₄ is to understand the roles played by chemical substitution in the creation of different multiferroic states. Different from Co doping, Cu [27] or Zn [24] doping produces an AF2 phase but not the AF5 phase. Why do different impurities stabilize different spiral states? There is ample evidence [39,40] that the SOI of Co has

a very different character than the SOI of Mn. The directional *L* = 1 orbital configurations of Co are quite different from the *L* = 0 configurations of Cu and Zn. However, at least for pure CoWO₄, the single-ion anisotropy of Co must have an easy-axis character to stabilize a collinear AF state [39]. In both MnWO₄ and CuFeO₂, the collinear spin state of the pure compounds is stabilized by the small, but important, easy-axis anisotropy with *K* > 0. A noncollinear and multiferroic state emerges when the single-ion anisotropy softens or changes sign. This may be a productive route to create multiferroic materials starting with 3*d*⁵ magnetic ions that exhibit *weak* easy-axis anisotropy.

In summary, we have performed systematic inelastic neutron scattering measurements to investigate the evolution of the SWs of multiferroic Mn_{1-x}Co_xWO₄ from the collinear AF1 phase to the *ac-b* spiral of the AF2 phase to the *ac* cycloid of the AF5 phase. SW excitations can be modeled by an effective Heisenberg model with competing long-range exchange interactions and the single-ion anisotropy *K*. While the chemical substitution drives the system from the collinear to the multiferroic spiral configuration, the dominant effect of doping is to reduce and switch the sign of *K* induced by the SOI, and the change in ratio of exchange constants remains minor.

ACKNOWLEDGMENTS

Research at ORNL’s SNS was sponsored by the Scientific User Facilities Division, Office of Basic Energy Sciences, U.S. Department of Energy. The theoretical work is sponsored by the U.S. Department of Energy, Office of Basic Energy Sciences, Materials Sciences and Engineering Division. Work at Houston is supported in part by the T.L.L. Temple Foundation, the John J. and Rebecca Moores Endowment, and the state of Texas through TCSUH, the U.S. Air Force Office of Scientific Research, Award No. FA9550-09-1-0656. J.C.W. acknowledges support from the China Scholarship Council. ORNL is managed by UT-Battelle, LLC, under Contract No. DE-AC05-00OR22725 for the U.S. Department of Energy.

-
- [1] T. Kimura, T. Goto, H. Shintani, K. Ishizaka, T. Arima, and Y. Tokura, *Nature (London)* **426**, 55 (2003).
 - [2] D. I. Khomskii, *J. Magn. Magn. Mater.* **306**, 1 (2006).
 - [3] S. W. Cheong and M. Mostovoy, *Nat. Mater.* **6**, 13 (2007).
 - [4] R. Ramesh and N. A. Spaldin, *Nat. Mater.* **6**, 21 (2007).
 - [5] Y. Tokura, *J. Magn. Magn. Mater.* **310**, 1145 (2007).
 - [6] Y. Tokura, S. Seki, and N. Nagaosa, *Rep. Prog. Phys.* **77**, 076501 (2014).
 - [7] H. Katsura, N. Nagaosa, and A. V. Balatsky, *Phys. Rev. Lett.* **95**, 057205 (2005).
 - [8] I. A. Sergienko and E. Dagotto, *Phys. Rev. B* **73**, 094434 (2006).
 - [9] M. Mostovoy, *Phys. Rev. Lett.* **96**, 067601 (2006).
 - [10] N. Hur, S. Park, P. A. Sharma, J. S. Ahn, S. Guha, and S.-W. Cheong, *Nature (London)* **429**, 392 (2004).
 - [11] C. Jia, S. Onoda, N. Nagaosa, and J. H. Han, *Phys. Rev. B* **74**, 224444 (2006).
 - [12] C. Jia, S. Onoda, N. Nagaosa, and J. H. Han, *Phys. Rev. B* **76**, 144424 (2007).
 - [13] K. Taniguchi, N. Abe, T. Takenobu, Y. Iwasa, and T. Arima, *Phys. Rev. Lett.* **97**, 097203 (2006).
 - [14] A. H. Arkenbout, T. T. M. Palstra, T. Siegrist, and T. Kimura, *Phys. Rev. B* **74**, 184431 (2006).
 - [15] O. Heyer, N. Hollmann, I. Klassen, S. Jodlauk, L. Bohaty, P. Becker, J. A. Mydosh, T. Lorenz, and D. Khomskii, *J. Phys.: Condens. Matter* **18**, L471 (2006).
 - [16] G. Lautenschlager, H. Weitzel, T. Vogt, R. Hock, A. Bohm, M. Bonnet, and H. Fuess, *Phys. Rev. B* **48**, 6087 (1993).
 - [17] I. Urcelay-Olabarria, J. M. Perez-Mato, J. L. Ribeiro, J. L.

- García-Munoz, E. Ressouche, V. Skumryev, and A. A. Mukhin, *Phys. Rev. B* **87**, 014419 (2013).
- [18] K. Taniguchi, N. Abe, H. Sagayama, S. Ohtani, T. Takenobu, Y. Iwasa, and T. Arima, *Phys. Rev. B* **77**, 064408 (2008).
- [19] H. Mitamura, T. Sakakibara, H. Nakamura, T. Kimura, and K. Kindo, *J. Phys. Soc. Jpn.* **81**, 054705 (2012).
- [20] I. Urcelay-Olabarria, E. Ressouche, A. A. Mukhin, V. Y. Ivanov, A. M. Kadomtseva, Y. F. Popov, G. P. Vorob'ev, A. M. Balbashov, J. L. García-Muñoz, and V. Skumryev, *Phys. Rev. B* **90**, 024408 (2014).
- [21] I. Urcelay-Olabarria, J. L. García-Muñoz, and A. A. Mukhin, *Phys. Rev. B* **91**, 104429 (2015).
- [22] F. Ye, Y. Ren, J. A. Fernandez-Baca, H. A. Mook, J. W. Lynn, R. P. Chaudhury, Y. Q. Wang, B. Lorenz, and C. W. Chu, *Phys. Rev. B* **78**, 193101 (2008).
- [23] L. Meddar, M. Josse, P. Deniard, C. La, G. André, F. Damay, V. Petricek, S. Jobic, M.-H. Whangbo, M. Maglione, and C. Payen, *Chem. Mater.* **21**, 5203 (2009).
- [24] R. P. Chaudhury, F. Ye, J. A. Fernandez-Baca, B. Lorenz, Y. Q. Wang, Y. Y. Sun, H. A. Mook, and C. W. Chu, *Phys. Rev. B* **83**, 014401 (2011).
- [25] H. W. Yu, M. F. Liu, X. Li, L. Li, L. Lin, Z. B. Yan, and J.-M. Liu, *Phys. Rev. B* **87**, 104404 (2013).
- [26] Y. S. Song, J. H. Chung, K. W. Shin, K. H. Kim, and I. H. Oh, *Appl. Phys. Lett.* **104**, 252904 (2014).
- [27] C. M. N. Kumar, Y. Xiao, P. Lunkenheimer, A. Loidl, and M. Ohl, *Phys. Rev. B* **91**, 235149 (2015).
- [28] J. Wang, F. Ye, S. Chi, J. A. Fernandez-Baca, H. Cao, W. Tian, M. Gooch, N. Poudel, Y. Wang, B. Lorenz, and C. W. Chu, *Phys. Rev. B* **93**, 155164 (2016).
- [29] F. Ye, S. Chi, J. A. Fernandez-Baca, H. Cao, K. C. Liang, Y. Wang, B. Lorenz, and C. W. Chu, *Phys. Rev. B* **86**, 094429 (2012).
- [30] Y.-S. Song, J.-H. Chung, J. M. S. Park, and Y.-N. Choi, *Phys. Rev. B* **79**, 224415 (2009).
- [31] Y.-S. Song, L. Q. Yan, B. Lee, S. H. Chun, K. H. Kim, S. B. Kim, A. Nogami, T. Katsufuji, J. Schefer, and J.-H. Chung, *Phys. Rev. B* **82**, 214418 (2010).
- [32] R. P. Chaudhury, F. Ye, J. A. Fernandez-Baca, Y. Q. Wang, Y. Y. Sun, B. Lorenz, H. A. Mook, and C. W. Chu, *Phys. Rev. B* **82**, 184422 (2010).
- [33] I. Urcelay-Olabarria, E. Ressouche, A. A. Mukhin, V. Y. Ivanov, A. M. Balbashov, J. L. García-Muñoz, and V. Skumryev, *Phys. Rev. B* **85**, 224419 (2012).
- [34] I. Urcelay-Olabarria, E. Ressouche, A. A. Mukhin, V. Y. Ivanov, A. M. Balbashov, G. P. Vorobev, Y. F. Popov, A. M. Kadomtseva, J. L. García-Muñoz, and V. Skumryev, *Phys. Rev. B* **85**, 094436 (2012).
- [35] N. Poudel, K. C. Liang, Y. Q. Wang, Y. Y. Sun, B. Lorenz, F. Ye, J. A. Fernandez-Baca, and C. W. Chu, *Phys. Rev. B* **89**, 054414 (2014).
- [36] N. Terada, T. Kawasaki, S. Mitsuda, H. Kimura, and Y. Noda, *J. Phys. Soc. Jpn.* **74**, 1561 (2005).
- [37] N. Terada, T. Nakajima, S. Mitsuda, H. Kitazawa, K. Kaneko, and N. Metoki, *Phys. Rev. B* **78**, 014101 (2008).
- [38] K.-C. Liang, Y.-Q. Wang, Y. Y. Sun, B. Lorenz, F. Ye, J. A. Fernandez-Baca, H. A. Mook, and C. W. Chu, *New J. Phys.* **14**, 073028 (2012).
- [39] N. Hollmann, Z. Hu, T. Willers, L. Bohaty, P. Becker, A. Tanaka, H. H. Hsieh, H. J. Lin, C. T. Chen, and L. H. Tjeng, *Phys. Rev. B* **82**, 184429 (2010).
- [40] Y.-S. Song, J.-H. Chung, S. H. Chun, K. H. Kim, and J. Schefer, *J. Phys. Soc. Jpn.* **82**, 124716 (2013).
- [41] N. L. Huang and R. Orbach, *Phys. Rev. Lett.* **12**, 275 (1964).
- [42] J. R. D. Copley and J. C. Cook, *Chem. Phys.* **292**, 477 (2003).
- [43] G. Ehlers, A. A. Podlesnyak, and A. I. Kolesnikov, *Rev. Sci. Instrum.* **87**, 093902 (2016).
- [44] R. T. Azuah, L. R. Kneller, Y. M. Qiu, P. L. W. Tregenna-Piggott, C. M. Brown, J. R. D. Copley, and R. M. Dimeo, *J. Res. Natl. Inst. Stand. Technol.* **114**, 341 (2009).
- [45] S. W. Lovesey, *Theory of Neutron Scattering from Condensed Matter* (Oxford University Press, Oxford, 1986), Vol. 2.
- [46] R. S. Fishman, J. Fernandez-Baca, and T. Rößm, *Spin-Wave Theory and Its Applications to Neutron Scattering and THz Spectroscopy* (Morgan and Claypool, San Rafael, CA, 2018).
- [47] F. Ye, R. S. Fishman, J. A. Fernandez-Baca, A. A. Podlesnyak, G. Ehlers, H. A. Mook, Y. Wang, B. Lorenz, and C. W. Chu, *Phys. Rev. B* **83**, 140401 (2011).
- [48] Y. Xiao, C. M. N. Kumar, S. Nandi, Y. Su, W. T. Jin, Z. Fu, E. Faulhaber, A. Schneidewind, and T. Brückel, *Phys. Rev. B* **93**, 214428 (2016).
- [49] I. V. Solovyev, *Phys. Rev. B* **87**, 144403 (2013).
- [50] J. T. Haraldsen, F. Ye, R. S. Fishman, J. A. Fernandez-Baca, Y. Yamaguchi, K. Kimura, and T. Kimura, *Phys. Rev. B* **82**, 020404 (2010).
- [51] S. H. Chun, K. W. Shin, H. J. Kim, S. Jung, J. Park, Y.-M. Bahk, H.-R. Park, J. Kyoung, D.-H. Choi, D.-S. Kim, G.-S. Park, J. F. Mitchell, and K. H. Kim, *Phys. Rev. Lett.* **120**, 027202 (2018).